Available online at www.sciencedirect.com
ScienceDirect
ELSEVIER
ISPRS Journal of Photogrammetry & Remote Sensing 62 (2007) 112–121
PHOTOGRAMMETRY & REMOTE SENSING
www.elsevier.com/locate/isprsjprs

Matching of 3D surfaces and their intensities ☆

Devrim Akca *

Institute of Geodesy and Photogrammetry, ETH Zurich, CH-8093 Zurich, Switzerland

Received 12 December 2005; received in revised form 27 May 2006; accepted 7 June 2006
Available online 14 July 2006

Abstract

3D surface matching would be an ill conditioned problem when the curvature of the object surface is either homogenous or isotropic, e.g. for plane or spherical types of objects. A reliable solution can only be achieved if supplementary information or functional constraints are introduced. In a previous paper, an algorithm for the least squares matching of overlapping 3D surfaces, which were digitized/sampled point by point using a laser scanner device, by the photogrammetric method or other techniques, was proposed [Gruen, A., and Akca, D., 2005. Least squares 3D surface and curve matching. ISPRS Journal of Photogrammetry and Remote Sensing 59 (3), 151–174.]. That method estimates the transformation parameters between two or more fully 3D surfaces, minimizing the Euclidean distances instead of z-differences between the surfaces by least squares. In this paper, an extension to the basic algorithm is given, which can simultaneously match surface geometry and its attribute information, e.g. intensity, colour, temperature, etc. under a combined estimation model. Three experimental results based on terrestrial laser scanner point clouds are presented. The experiments show that the basic algorithm can solve the surface matching problem provided that the object surface has at least the minimal information. If not, the laser scanner derived intensities are used as supplementary information to find a reliable solution. The method derives its mathematical strength from the least squares image matching concept and offers a high level of flexibility for many kinds of 3D surface correspondence problem.

Keywords: surface matching; least squares matching; point clouds; registration; laser scanning; intensity matching; attribute information

1. Introduction

For 3D object modelling, data acquisition must be performed from different standpoints. The derived local point clouds must be transformed into a common system. This procedure is usually referred to as registration. In the literature, several attempts have been described concerning the registration of 3D point clouds. One of the most popular methods is the Iterative Closest Point (ICP) algorithm developed by Besl and McKay (1992), Chen and Medioni (1992) and Zhang (1994). The ICP is based on the search for pairs of nearest points in the two sets and estimates the rigid body transformation that aligns them. Then, the rigid body transformation is applied to the points of one set and the procedure is iterated until convergence is achieved.

In Besl and McKay (1992) and Zhang (1994) the ICP requires every point in one surface to have a corresponding point on the other surface. Alternatively, the distance between the transformed points in one

☆ Upgraded and modified version of a paper presented at the XXth ISPRS Congress in Istanbul, July 2004.

* Tel.: +41 1 633 3063; fax: +41 1 633 1101.
E-mail address: akca@geod.baug.ethz.ch.

0924-2716/$ - see front matter © 2006 International Society for Photogrammetry and Remote Sensing, Inc. (ISPRS). Published by Elsevier B.V. All rights reserved.
doi:10.1016/j.isprsjprs.2006.06.001

surface and corresponding tangent planes on the other surfaces was used as a registration evaluation function (Chen and Medioni, 1992; Bergevin et al., 1996; Pulli, 1999). The point-to-tangent plane approach gives a better registration accuracy than the point-to-point approach.

The parameters of the rigid body transformation are generally estimated by the use of closed-form solutions, mainly singular value decomposition and quaternion methods. Eggert et al. (1997) and Williams et al. (1999) provide an extensive review and comparison. The closed-form solutions cannot fully consider the statistical point error models. Zhang (1994) and Dorai et al. (1997) weighted the individual points based on a priori noise information. Williams et al. (1999), Guehring (2001) and Okatani and Deguchi (2002) proposed methods that can model the anisotropic point errors.

The gradient descent type of algorithms can support full stochastic models for measurement errors, and assure a substantially lower number of iterations than the ICP variants (Szeliski and Lavallee, 1996; Neugebauer, 1997; Fitzgibbon, 2001). The Levenberg–Marquardt method is usually adopted for the estimation.

The ICP, and in general all surface registration methods, requires heavy computations. Strategies employed to reduce the computation time are: reduction of the number of iterations, reduction of the number of employed points, and speeding up the correspondence computation. Extensive surveys on commonly used methods are given in Jost and Huegli (2003), Park and Subbarao (2003) and Akca and Gruen (2005).

Several reviews and comparison studies on surface registration methods are available in the literature (Jokinen and Haggren, 1998; Williams et al., 1999; Campbell and Flynn, 2001; Rusinkiewicz and Levoy, 2001; Gruen and Akca, 2005).

When the surface curvature is either homogeneous or isotropic, as is the case with all first or second order surfaces, e.g. plane or spherical surfaces, the geometry-based registration techniques will fail. In some studies, surface geometry and intensity (or colour) information have been combined in order to solve this problem. Maas (2001) used the airborne laser scanner reflectance images as complimentary to the height data for the determination of horizontal shift parameters between the laser scanner strips of flat areas. Roth (1999) and Vanden Wyngaerd and Van Gool (2003) used feature-based methods in which interest points and regions are extracted from the intensity images. More often the intensity information is processed as an extra distance value under an ICP algorithm in order to reduce the search effort for corresponding point pairs or in order to eliminate the ambiguities due to inadequate geometric information on the object surface (Weik, 1997; Johnson and Kang, 1999; Godin et al., 2001; Yoshida and Saito, 2002).

In a previous work, an algorithm for the least squares matching of overlapping 3D surfaces, called Least Squares 3D Surface Matching (LS3D), was proposed (Gruen and Akca, 2005). It estimates the transformation parameters between two or more fully 3D surfaces, using the Generalized Gauss–Markoff model, minimizing the sum of the squares of the Euclidean distances between the surfaces. This formulation gives the opportunity of matching arbitrarily oriented 3D surfaces simultaneously, without using explicit tie points. The mathematical model introduced in this paper is a generalization of the least squares image matching method, in particular the method given by Gruen (1985). For the details of the mathematical modelling and execution aspects, the reader is referred to Gruen and Akca (2005).

When the object surface lacks sufficient geometric information, i.e. homogeneity or isotropicity of curvatures, the basic algorithm will either fail or find a side minimum. This work proposes a solution in which available attribute information, e.g. intensity, colour, temperature, etc., is used to form quasisurfaces in addition to the actual ones. The matching is performed by simultaneous use of surface geometry and attribute information under a combined estimation model. The formation of the quasisurfaces and mathematical modelling of the problem are given in the following section. The experimental results based on terrestrial laser scanner point clouds are presented in the third section.

2. Simultaneous matching of surface geometry and intensity

2.1. Problem definition

$f(x, y, z)$, being the template surface, is a discrete 3D function, which represents an object surface. $g(x, y, z)$, being the search surface, is its conjugate part, which was digitized from a different viewpoint or at a different time or by a different sensor. Every sampled element of the template and the search surfaces has an attribute value in addition to the 3D coordinates.

Matching is established in an ideal case:

$$f(x,y,z) = g(x,y,z) \tag{1}$$

Because of the effects of random error, Eq. (1) is not consistent. Therefore, a true error vector $e(x, y, z)$ is

added, assuming that the template noise is independent of the search noise.

$$f(x,y,z)-e(x,y,z)=g(x,y,z) \tag{2}$$

The problem is estimating the parameters of a 3D transformation, which satisfies the least squares matching of the search surface $g(x, y, z)$ to the template $f(x, y, z)$. This is achieved by minimizing a goal function, which measures the sum of the squares of the Euclidean distances between the surfaces.

In order to perform a least squares estimation, Eq. (2) is expanded using the Taylor series, of which only the linear terms are retained:

$$-e(x,y,z)=\frac{\partial g^0(x,y,z)}{\partial x}\mathrm{d}x+\frac{\partial g^0(x,y,z)}{\partial y}\mathrm{d}y+\frac{\partial g^0(x,y,z)}{\partial z}\mathrm{d}z-(f(x,y,z)-g^0(x,y,z)) \tag{3}$$

with notations

$$g_x=\frac{\partial g^0(x,y,z)}{\partial x},\quad g_y=\frac{\partial g^0(x,y,z)}{\partial y},\quad g_z=\frac{\partial g^0(x,y,z)}{\partial z} \tag{4}$$

where the terms $\{g_x, g_y, g_z\}$ are the numerical first derivatives of the function $g(x, y, z)$ and the terms $\{\mathrm{d}x, \mathrm{d}y, \mathrm{d}z\}$ are the differentiation of the selected 3D transformation model. A 7-parameter 3D similarity transformation is used for the geometric relationship.

After further expansions, Eq. (3) gives in matrix notation

$$-\boldsymbol{e}=\mathbf{A}\boldsymbol{x}-\boldsymbol{l},\quad \mathbf{P} \tag{5}$$

where $\mathbf{A}$ is the design matrix, $\boldsymbol{x}$ is the parameter vector which here contains three translation, one scale and three rotation parameters, $\mathbf{P}=\mathbf{P}_{ll}$ is the a priori weight matrix, and $\boldsymbol{l}=f(x, y, z)-g^0(x, y, z)$ is the discrepancy vector that consists of the Euclidean distances between the template and correspondent search surface elements.

The parameters are introduced into the system as observables with the associated weight coefficient matrix $\mathbf{P}_b$.

$$-\boldsymbol{e}_b=\mathbf{I}\boldsymbol{x}-\boldsymbol{l}_b,\quad \mathbf{P}_b \tag{6}$$

where $\mathbf{I}$ is the identity matrix and $\boldsymbol{l}_b$ is the (fictitious) observation vector. The joint system equations (5) and (6) are solved by applying the least squares criteria. The reader is referred to Gruen and Akca (2005) for details of the derivation and solution of Eqs. (5) and (6).

When there is a lack of sufficient geometric information (homogeneity or isotropicity of curvatures), the procedure may fail, since there is not a unique solution geometrically, e.g. when matching two planes or spherical objects. An object surface may have some attribute information attached to it. Intensity, colour and temperature are well known examples. Most of the laser scanners can supply intensity information in addition to the Cartesian coordinates for each point, or an additional camera may be used to collect texture. A solution is proposed that can simultaneously match intensity information and geometry under a combined estimation model. In this approach the intensity image of the point cloud also contributes observation equations to the system, considering the intensities as supplementary information to the range image.

2.2. Formation of quasisurfaces

Rather than adopting a feature-based or step-wise approach, this method sets up quasisurfaces from intensity information in addition to the actual surfaces.

Surface representation is carried out in two different forms; triangle and grid mesh forms. Both of these are first degree C^0 continuous representations. Surface topology is established simply by reading the standard laser scanner output files in ASCII format and loading them in the scan-line order.

A hypothetical example of forming the quasisurfaces is given in Fig. 1. The procedure starts with the calculation of surface normal vectors at each data point. The actual surface will include noise and surface spikes (Fig. 1b), which lead to unrealistic calculations for the normal vectors. To cope with the problem, a moving average or median type filtering process could be employed. But still some noise would remain depending on the window size.

An optimum solution is the least squares fitting of a global trend surface to the whole point cloud (Fig. 1c). It will suppress the noise component and preserve the global continuity of the normal vectors along the surface. The parametric bi-quadratic trend surface was chosen, which is sufficient to model the quadric type of surfaces, e.g. plane, sphere, ellipsoid, etc. For the template surface patch $f(x, y, z)$:

$$F(u,w)=\sum_{i=0}^{2}\sum_{j=0}^{2}\boldsymbol{b}_{ij}u^i w^j \tag{7}$$

where $u, w\in[0,1]^2$, $F(u,w)\in\mathcal{R}^3$ is the position vector of any point on the trend surface, and $\boldsymbol{b}_{ij}\in\mathcal{R}^3$ are the algebraic coefficients, which are estimated by least squares fitting.

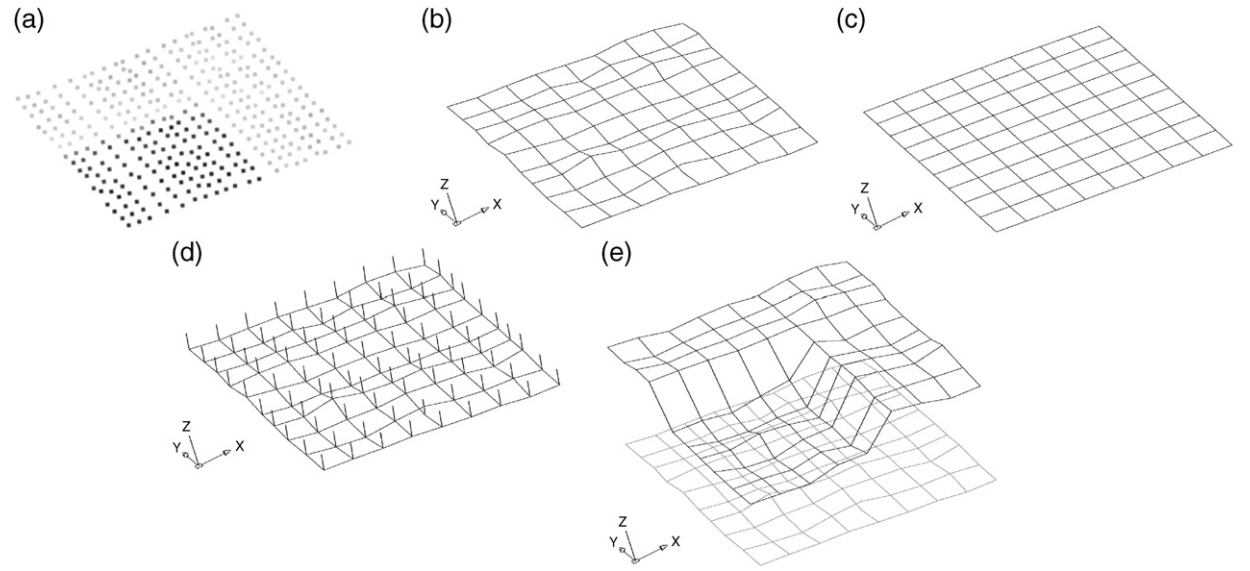

Fig. 1. Forming the quasisurface. (a) Point cloud with intensity information, (b) meshed surface of the point cloud, (c) trend surface fitted to the point cloud, (d) normal vectors attached onto the actual surface, and (e) generated quasisurface in addition to the actual one.

For each point, the normal vector $\boldsymbol{n}_f$ is calculated on the trend surface $F(u,w)$ and attached to the actual surface $f(x, y, z)$ (Fig. 1d):

$$\boldsymbol{n}_f = \boldsymbol{n}_f(u,w) = \frac{\boldsymbol{F}_u \times \boldsymbol{F}_w}{||\boldsymbol{F}_u \times \boldsymbol{F}_w||} \tag{8}$$

where $\boldsymbol{F}_u$ and $\boldsymbol{F}_w$ are the tangent vectors along the u and w-axes, respectively.

Finally, the quasisurface $f_c(x, y, z)$ is formed in such a way that each point of the actual surface $f(x, y, z)$ is mapped along its normal vector $\boldsymbol{n}_f$ up to a distance proportional to its intensity value c_f (Fig. 1e).

$$f_c(x,y,z) = f(x,y,z) + \boldsymbol{n}_f \lambda c_f \tag{9}$$

where λ is an appropriate scalar factor for the conversion from the intensity range to the Cartesian space.

Rather than the actual surface $f(x, y, z)$, the trend surface $F(u,w)$ can also be defined as the datum, which leads to

$$f_c(x,y,z) = F(u,w) + \boldsymbol{n}_f \lambda c_f \tag{10}$$

This isolates the geometric noise component from the quasisurface $f_c(x, y, z)$, but strongly smoothes the geometry.

Eqs. (9) and (10) assume a fairly simplistic radiometric model (intensities are mapped perpendicular to the geometric surface). This model can be refined by considering an appropriate illumination model.

The same procedure is performed for the search surface $g(x, y, z)$ as well:

$$g_c(x,y,z) = g(x,y,z) + \boldsymbol{n}_g \lambda c_g \tag{11}$$

2.3. The estimation model

Eq. (2) should also be valid for the quasisurfaces under the assumption that similar illumination conditions exist for both the template and search surfaces:

$$f_c(x,y,z) - e_c(x,y,z) = g_c(x,y,z) \tag{12}$$

The random errors of the template and search quasisurfaces are assumed to be uncorrelated. The contrast and brightness differences or in the extreme case specular reflection will cause model errors, and deteriorate the reliability of the estimation. The radiometric variations between the template and search surface intensities should be reduced before matching by pre-processing or appropriate modelling in the estimation process by the use of extra parameters.

For two images of an object acquired by an optical-passive sensor, e.g. a CCD camera, an intensity transfer function such as ($c_f = r_0 + c_g r_1$) could be suitable for the radiometric adaptation, where r_0 (shift) and r_1 (scale) are radiometric correction parameters. In the case of laser scanner derived intensity images, the radiometric variations are strongly dependent on both the incident angle of the signal path with respect to the normal to the

object surface and the object-to-sensor distance. Thus, for a plane type of object, the radiometric variations can be modelled in first approximation as in the following:

$$f_c(x,y,z)-e_c(x,y,z) = g_c(x,y,z) + r_0 + ur_1 \tag{13}$$

where u is the abscissa of the search trend surface $G(u,w)$, considering that the u-axis is the horizontal direction. In other words, the u-axis is the principal direction of change of the incident angles. Depending on the characteristics of the scan data, it can be replaced by ordinate value w, or another type of parameterization. In general a second order bivariate polynomial ($r_0+ur_1+wr_2+uwr_3+u^2r_4+w^2r_5+u^2wr_6+uw^2r_7+u^2w^2r_8$) or an appropriate subpart of it can be used.

Although the radiometric parameters r_0 and r_1 are linear a priori, they are expanded using the Taylor series. Eq. (13) in linearized form gives:

$$\begin{aligned}-e_c(x,y,z) = {} & \frac{g_c^0(x,y,z)}{\partial x}\mathrm{d}x + \frac{g_c^0(x,y,z)}{\partial y}\mathrm{d}y \\ & + \frac{g_c^0(x,y,z)}{\partial z}\mathrm{d}z + \mathrm{d}r_0 + u\mathrm{d}r_1 - (f_c(x,y,z) \\ & - g_c^0(x,y,z) - \{r_0^0 + ur_1^0; \boldsymbol{n}_g\})\end{aligned} \tag{14}$$

with notations

$$g_{cx} = \frac{\partial g_c^0(x,y,z)}{\partial x}, \quad g_{cy} = \frac{\partial g_c^0(x,y,z)}{\partial y}, \quad g_{cz} = \frac{\partial g_c^0(x,y,z)}{\partial z} \tag{15}$$

where the terms $\{g_{cx}, g_{cy}, g_{cz}\}$ stand for the numerical derivatives of the quasi-search surface function. The first approximations of the radiometric parameters are $r_0^0=r_1^0=0$. At the end of each iteration, the quasi-search surface $g_c^0(x, y, z)$ is transformed to a new state using the updated set of transformation parameters, and subsequently re-shaped by the current set of radiometric parameters $r_0^0+ur_1^0$ along the normal vectors $\boldsymbol{n}_g$, which are calculated on the search trend surface $G(u,w)$.

The terms $\{\mathrm{d}x, \mathrm{d}y, \mathrm{d}z\}$ relate Eqs. (3) and (14) to each other.

The quasisurfaces are treated like actual surfaces in the estimation model. They contribute observation equations to the design matrix, joining the system by the same set of transformation parameters. After further expansion and with the assumptions $E\{\boldsymbol{e}_c\}=0$ and $E\{\boldsymbol{e}_c\ \boldsymbol{e}_c^{\mathrm{T}}\}=\sigma_0^2\mathbf{P}_c^{-1}$, Eq. (14) becomes

$$-\boldsymbol{e}_c = \mathbf{A}_c\boldsymbol{x}-\boldsymbol{l}_c, \quad \mathbf{P}_c \tag{16}$$

where $\boldsymbol{e}_c$, $\mathbf{A}_c$, $\boldsymbol{x}$, and $\mathbf{P}_c$ are the true error vector, the design matrix, the parameter vector, and the associated weight coefficient matrix for the quasisurface observations, respectively, and $\boldsymbol{l}_c$ is the constant vector that contains the Euclidean distances between the template and corresponding search quasisurface elements. Here, the vector $\boldsymbol{x}$ is extended to include the radiometric parameters in addition to the transformation parameters.

The hybrid system in Eqs. (5), (6) and (16) is of the combined adjustment type that allows simultaneous matching of geometry and intensity. The least squares solution of the system gives

$$\begin{aligned}\hat{\boldsymbol{x}} = {} & (\mathbf{A}^{\mathrm{T}}\mathbf{P}\mathbf{A} + \mathbf{P}_b + \mathbf{A}_c^{\mathrm{T}}\mathbf{P}_c\mathbf{A}_c)^{-1}(\mathbf{A}^{\mathrm{T}}\mathbf{P}\boldsymbol{l} + \mathbf{P}_b\boldsymbol{l}_b \\ & + \mathbf{A}_c^{\mathrm{T}}\mathbf{P}_c\boldsymbol{l}_c)\end{aligned} \tag{17}$$

In the experiments, weights for the quasisurface observations are selected as $(\mathbf{P}_c)_{ii}<(\mathbf{P})_{ii}$, and the intensity measurements of the (laser) sensor are considered to be uncorrelated with the distance measurements ($E\{\boldsymbol{e}_c\ \boldsymbol{e}^{\mathrm{T}}\}=0$) for the sake of simplicity of the stochastic model.

3. Experimental results

Three practical examples are given to show the capabilities of the method. Although the first example does not utilize the attribute information, it does serve to discuss the optimism of the precision estimates. The last two examples show the advantage of the joint use of surface geometry and attribute information.

All experiments were carried out using self-developed C/C++ software that runs on Microsoft Windows® OS. In all experiments the initial approximations of the unknowns were provided by interactively selecting 3 common points on both surfaces before matching. Since in all data sets there was no scale difference, the scale factor was fixed to unity. The iteration criteria values were selected for the elements of the translation vector as 1.0e−4 m in the "plant" example, and 2.0e−4 m in the "ball" and "wall painting" examples and for the rotation angles 1.0e−3 gon in the "plant" example, and 5.0e−3 gon in the "ball" and "wall painting" examples. They vary according to the unit and resolution of the data and size of the object volume.

The first example is the registration of three point clouds of an industrial plant (Fig. 2). The scanning was performed by the HDS 2500 (Leica Geosystems) laser scanner. The average point spacing is 12 mm. The first and third point clouds (Fig. 2a and c) were matched to the second one (Fig. 2b) using the basic algorithm of the LS3D surface matching method. The numerical results of the matching of the first and third point clouds are given in parts I and II of Table 1, respectively. In Table 1,

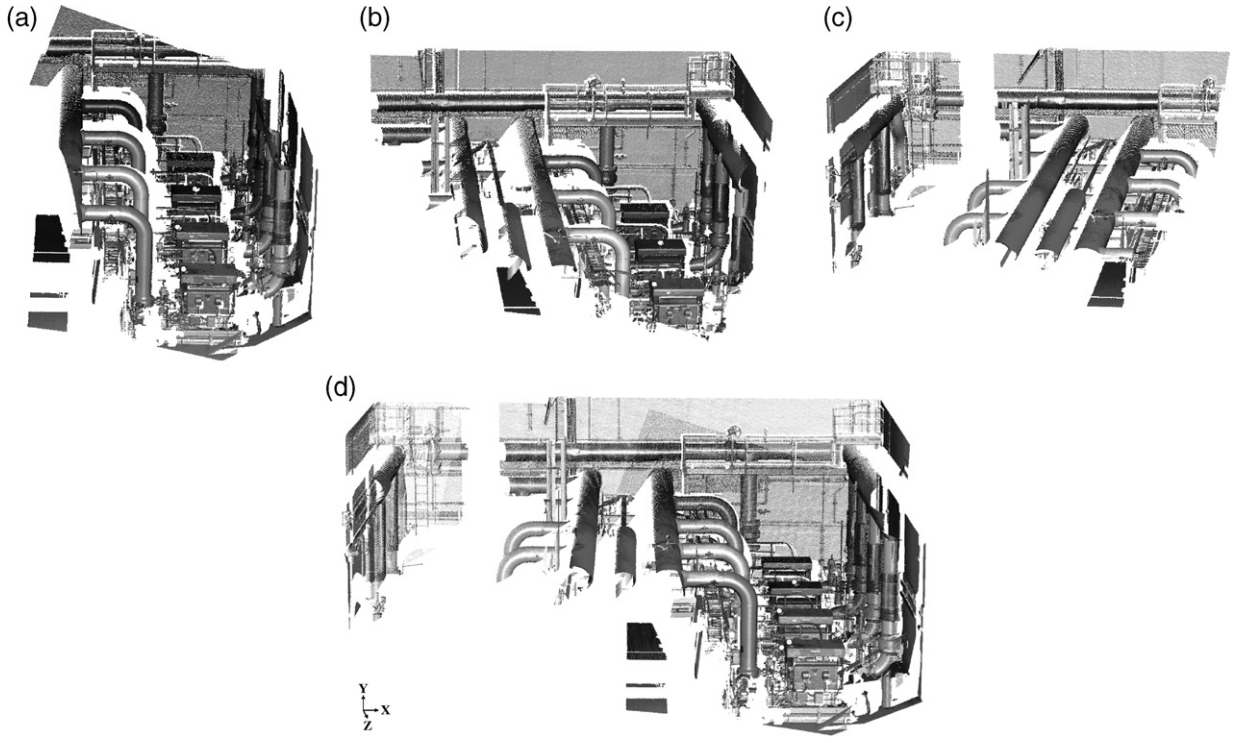

Fig. 2. Example of "plant". (a), (b), (c) First, second and third point cloud, and (d) composite point cloud after the LS3D surface matching. Note that laser scanner derived intensities are back-projected onto the point clouds only for the purpose of visualization.

"No. of points" column stands for the number of the remaining correspondences at the last iteration, resulting from a simple robust estimation principle, which aims to eliminate only the large outliers and occlusions. More details can be found in Gruen and Akca (2005).

Even though it is a very complex environment with many occlusions, the matching process is successful. Small magnitudes of the theoretical precisions of the parameters indicate a proper fit along all directions. This example shows that the basic algorithm can successfully find the solution in the presence of sufficient surface geometry.

However, the theoretical precisions are optimistic. They are much beyond the accuracy limit of the sensor. In order to see the effect of the redundancy on the theoretical precision values, a further matching process was carried out. Rather than the whole overlapping areas, occlusion-free cooperative sub-patches were matched. The results are given in parts I″ and II″ of Table 1. Although the precision values increased, they are still

Table 1
Numerical results of "plant" example

#	Surface type	No. of points	No. of observation equations ($n_l+n_b+n_c$)	No. of iterations	$\hat{\sigma}_0$ (mm)	$\hat{\sigma}_{tx}/\hat{\sigma}_{ty}/\hat{\sigma}_{tz}$ (mm)	$\hat{\sigma}_\omega/\hat{\sigma}_\varphi/\hat{\sigma}_\kappa$ (1.0e−02 gon)
I	P	245041	245041+7+0	6	2.78	0.03 / 0.03 / 0.01	0.01 / 0.01 / 0.03
	B			5	2.79	0.03 / 0.03 / 0.01	0.01 / 0.01 / 0.03
II	P	323936	323936+7+0	7	2.54	0.02 / 0.02 / 0.01	0.01 / 0.01 / 0.02
	B			6	2.52	0.02 / 0.02 / 0.01	0.01 / 0.01 / 0.02
I″	P	20407	20407+7+0	6	2.11	0.09 / 0.09 / 0.04	0.05 / 0.04 / 0.08
	B			5	2.09	0.09 / 0.09 / 0.04	0.05 / 0.04 / 0.08
II″	P	37983	37983+7+0	8	2.01	0.04 / 0.04 / 0.02	0.03 / 0.03 / 0.07
	B			8	2.00	0.04 / 0.05 / 0.02	0.03 / 0.03 / 0.07

P: Plane surface representation in triangle mesh form.
B: Bi-linear surface representation in grid mesh form.
n_l, n_b, n_c: Number of observation equations for actual surfaces, parameters and quasisurfaces, respectively.

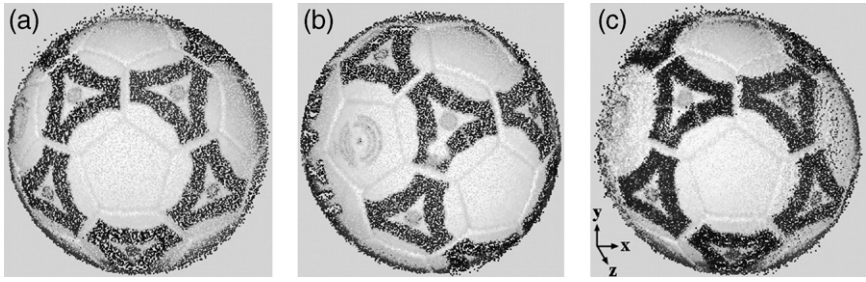

Fig. 3. Example of "ball". (a) The search point cloud, (b) the template point cloud, and (c) the composite point cloud after the combined matching of geometry and intensity. Note that laser scanner derived intensities are back-projected onto the point clouds.

optimistic, mainly due to the stochastic properties of the search surfaces that have not been considered as such in the estimation model, as is typically done in least squares matching. The omissions are expected to be minor and do not disturb the solution vector significantly. However, the a posteriori covariance matrix will be affected by the neglected uncertainty of the function values $g(x, y, z)$. This deteriorates the realistic precision estimates. More details on this issue can be found in Gruen (1985), Maas (2002) and Gruen and Akca (2005).

The second experiment refers to simultaneous matching of surface geometry and intensity. A soccer ball (Fig. 3) was scanned using the IMAGER 5003 (Zoller+Fröhlich) laser scanner. The average point spacing is 2 mm. Laser scanner derived reflectance values were used as intensity information. The intensities of the template and search surfaces were adapted by pre-processing prior to the matching. However, it was not possible to fully adjust the radiometric variations. This degrades the quality of the quasisurfaces. The actual surface observations were considered as the unit weight $(\mathbf{P})_{ii}=1.00$. Consequently, weights for the quasisurfaces observations were selected as $(\mathbf{P}_c)_{ii}=0.20$. The numerical results are given in part III of Table 2. In Table 2, the numbers of equations for the actual surface and quasisurface observations differ. Although they are the same at the beginning, during the iteration observations of the actual and quasisurfaces containing gross errors, are excluded by the aforementioned robust estimation principle, resulting in a different number of equations for the two surfaces.

The slow convergence and slightly high standard deviation values are the result of the low data quality. Actually, the test object is not suitable for measuring by a medium-range laser scanner due to its non-diffuse reflectance property. This caused noisy and erroneous points in the range data, especially along the object silhouettes, and specular reflections in the intensity data.

For the purpose of comparison, the same experiment was run with the only surface geometry option of the LS3D matching method. An identical solution vector was found but apparently with poorer theoretical precision values: for the translation parameters 2.30, 2.89 and 1.47 mm and for the rotation angles 26.70^c, 18.09^c and 16.04^c along the x–y–z axes, respectively (part III″ of Table 2). In fact, the test object does not have an ideal spherical shape. The shallow slots at the junctions of the pentagon parts of the ball (Fig. 3) prevent the failure of the only surface geometry option.

The last experiment is the matching of two partial scans of a wall painting in Neuschwanstein Castle in Bavaria, Germany (Fig. 4). The scanning was performed using the IMAGER 5003 terrestrial laser scanner. The average point spacing is 5 mm. The search surface (Fig. 4a) was matched to the template one (Fig. 4b) by simultaneous use of surface

Table 2
Numerical results of "ball" example

#	Surface type	No. of points	No. of observation equations ($n_l+n_b+n_c$)	No. of iterations	RMSE (mm)	$\hat{\sigma}_{tx}/\hat{\sigma}_{ty}/\hat{\sigma}_{tz}$ (mm)	$\hat{\sigma}_{\omega}/\hat{\sigma}_{\varphi}/\hat{\sigma}_{\kappa}$ (1.0e−02 gon)
III[a]	P	2548	2548+7+2617	12	1.14	1.20 / 1.56 / 0.81	14.54 / 9.68 / 9.27
	B			14	1.11	1.16 / 1.46 / 0.78	13.92 / 9.26 / 8.88
III″	P	2589	2589+7+0	21	1.70	2.30 / 2.89 / 1.47	26.70 / 18.09 / 16.04
	B			22	1.50	2.02 / 2.62 / 1.31	24.40 / 15.66 / 13.91

RMSE: root mean square error of the residuals of the actual surface observations.
[a] Datum is the actual surface f/g (x, y, z).

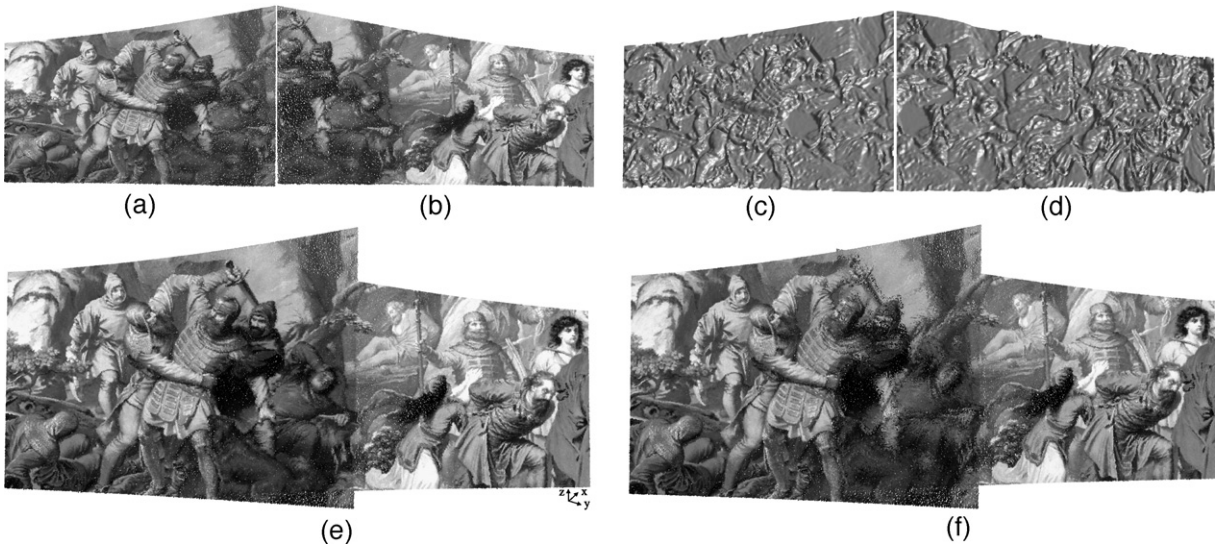

Fig. 4. Example of "wall painting". Actual (a) search and (b) template surfaces, generated (c) quasi-search and (d) quasi-template surfaces, (e) composite point cloud after the simultaneous matching of geometry and intensity by LS3D, and (f) result of matching of only surface geometry by LS3D. Note that laser scanner derived intensities are back-projected onto the point clouds (a), (b), (e) and (f).

geometry and intensity information. Laser scanner derived reflectance values were used as intensity information. The weights were selected for the actual surface observations as $(\mathbf{P})_{ii}=1.00$ and for the quasisurface observations as $(\mathbf{P}_c)_{ii}=0.75$. The numerical results are given in parts IV and V of Table 3.

Since the object is a plane, surface geometry alone is not enough for the matching. Using the combined approach of matching surface geometry and intensity of the LS3D, a successful solution has been achieved. The generated quasisurfaces (Fig. 4c and d) have been used in addition to the actual ones (Fig. 4a and b) in the matching process. The radiometric variations between the template and search surface intensities were modelled in the estimation by two extra parameters r_0 (shift) and r_1 (scale). The use of the trend surface as datum gives a slightly better convergence rate.

Another comparison has been made by matching the same data set using the basic algorithm of the LS3D surface matching method. It immediately converged to the closest local minimum of the initial approximations, hence to a false solution. The existing noise in the data avoids the singularity of the normal equations matrix. Although the matching along the depth direction is correct, there is an incorrect solution along the lateral direction due to ambiguity of the surface information (Fig. 4f). The theoretical precisions are slightly worse than those given in parts IV and V of Table 3, i.e. 0.03, 0.22 and 0.16 mm for the translation parameters and 0.37^c, 0.35^c and 0.46^c for the rotation angles along the x–y–z axes, respectively (part V″ of Table 3). The differences are not significant, but consistent. The depth direction related parameters t_x, t_y and κ show almost the same values with respect to the values produced by the joint use of surface geometry and

Table 3
Numerical results of "wall painting" example

#	Surface type	No. of points	No. of observation equations ($n_l+n_b+n_c$)	No. of iterations	RMSE (mm)	$\hat{\sigma}_{tx}/\hat{\sigma}_{ty}/\hat{\sigma}_{tz}$ (mm)	$\hat{\sigma}_{\omega}/\hat{\sigma}_{\varphi}/\hat{\sigma}_{\kappa}$ (1.0e−02 gon)
IV[a]	P	31 859	31 859+9+31 852	14	1.67	0.02 / 0.21 / 0.12	0.28 / 0.25 / 0.46
	B			13	1.72	0.02 / 0.21 / 0.12	0.29 / 0.26 / 0.44
V[b]	P	31 858	31 858+9+31 843	13	1.68	0.02 / 0.19 / 0.11	0.25 / 0.23 / 0.41
	B			12	1.73	0.02 / 0.19 / 0.11	0.26 / 0.24 / 0.40
V″	P	31 842	31 842+7+0	4	1.72	0.03 / 0.22 / 0.16	0.37 / 0.35 / 0.46
	B			3	1.77	0.03 / 0.21 / 0.18	0.42 / 0.38 / 0.45

[a] Datum is the actual surface f/g (x, y, z).
[b] Datum is the trend surface F/G (u,w).

intensity, as expected, whereas the lateral direction related parameters obviously have greater magnitude.

4. Conclusions

Least squares image matching is a fundamental measurement algorithm, and has been applied to a great variety of data matching problems due to its strong mathematical model. One of its straightforward extensions, applied to 3D object matching, is multiple cuboid matching in 3D voxel space (Maas, 1994; Maas and Gruen, 1995). In a previous work, it was employed for the 3D surface matching case (Gruen and Akca, 2005). In this paper, a method is proposed, based on the previous work, for the co-registration of surfaces whose curvature is either homogeneous or isotropic.

The proposed method accommodates the available attribute information and surface geometry under a combined estimation model. If available, any kind of functional constraint can also be introduced to the system. The attribute information is utilized by generating the quasisurfaces in addition to the actual ones. Any type of attribute information contributes one more quasisurface layer to the data. Therefore, it generalizes the problem to matching of isosurfaces rather than single surfaces.

The least squares concept allows for the monitoring of the quality of the final results by means of precision and reliability criteria. These measures give a quantitative insight into the data content, and help to assess the success level of the solution. Experiments show that as long as the object surface has minimal information, e.g. very small structures on it, the basic algorithm, which uses only surface geometry, can find an acceptable solution. When the object surface is a plane or quadric, the surface geometry approach does not numerically fail as the sensor noise prevents the normal equation matrix from becoming singular. However, it finds a side minimum as the solution. In this case, the proposed method can find a reliable solution by introducing supplementary attribute information into the system. In the experiments, the laser scanner derived intensities were used as the supplementary information. The practical examples demonstrate the capability of the technique. Special attention should be paid to the radiometric variations between the surfaces. Additional radiometric correction parameters have been added to the mathematical model. This gives better results than the pre-processing option.

The concept is not restricted to the registration of laser scanner point clouds. It can find more application areas for cases where diverse types of attribute information are used.

Acknowledgements

I would like to thank Mr. Martin Vögele (Leica Geosystems AG, Zurich, Switzerland) and Mr. Peter Glueck (Leica Geosystems HDS Inc., Rijswijk, The Netherlands) for providing the "plant" data set, Mr. Thorsten Schulz (Institute of Geodesy and Photogrammetry, ETH Zurich, Switzerland) for providing the "ball" data set, and Mr. Thomas Abmayr (Zoller+Fröhlich GmbH Elektrotechnik, Wangen, Germany) for providing the "wall painting" data set. I would like to express my gratitude to my advisor, Prof. Armin Gruen, for his invaluable advice and support on the work presented here. The author is financially supported by an ETHZ internal research grant, which is gratefully acknowledged. The author appreciates the ISPRS for supporting young scientists and students by preparing a special issue of the journal, which was initiated by the previous Editor Dr. Emmanuel Baltsavias and XXth ISPRS Congress Director Prof. Orhan Altan and carried out by the current Editor Prof. George Vosselman. Lastly, special thanks go to Prof. George Vosselman for his valuable criticism and suggestions that improved this paper.

References

Akca, D., Gruen, A., 2005. Fast correspondence search for 3D surface matching. International Archives of Photogrammetry, Remote Sensing and Spatial Information Sciences 36 (Part 3/W19), 186–191.

Bergevin, R., Soucy, M., Gagnon, H., Laurendeau, D., 1996. Towards a general multi-view registration technique. IEEE Transactions on Pattern Analysis and Machine Intelligence 18 (5), 540–547.

Besl, P.J., McKay, N.D., 1992. A method for registration of 3D shapes. IEEE Transactions on Pattern Analysis and Machine Intelligence 14 (2), 239–256.

Campbell, R.J., Flynn, P.J., 2001. A survey of free-form object representation and recognition techniques. Computer Vision and Image Understanding 81 (2), 166–210.

Chen, Y., Medioni, G., 1992. Object modelling by registration of multiple range images. Image and Vision Computing 10 (3), 145–155.

Dorai, C., Weng, J., Jain, A.K., 1997. Optimal registration of object views using range data. IEEE Transactions on Pattern Analysis and Machine Intelligence 19 (10), 1131–1138.

Eggert, D.W., Lorusso, A., Fisher, R.B., 1997. Estimating 3-D rigid body transformations: a comparison of four major algorithms. Machine Vision and Applications 9 (5–6), 272–290.

Fitzgibbon, A.W., 2001. Robust registration of 2D and 3D point sets. British Machine Vision Conference, Manchester, September 10–13, pp. 411–420.

Godin, G., Laurendeau, D., Bergevin, R., 2001. A method for the registration of attributed range images. IEEE International Conference on 3D Digital Imaging and Modeling, Quebec, May 28–June 1, pp. 179–186.

Gruen, A., 1985. Adaptive least squares correlation: a powerful image matching technique. South African Journal of Photogrammetry, Remote Sensing and Cartography 14 (3), 175–187.

Gruen, A., Akca, D., 2005. Least squares 3D surface and curve matching. ISPRS Journal of Photogrammetry and Remote Sensing 59 (3), 151–174.

Guehring, J., 2001. Reliable 3D surface acquisition, registration and validation using statistical error models. IEEE International Conference on 3D Digital Imaging and Modeling, Quebec, May 28–June 1, pp. 224–231.

Johnson, A.E., Kang, S.B., 1999. Registration and integration of textured 3D data. Image and Vision Computing 17 (2), 135–147.

Jokinen, O., Haggren, H., 1998. Statistical analysis of two 3-D registration and modeling strategies. ISPRS Journal of Photogrammetry and Remote Sensing 53 (6), 320–341.

Jost, T., Huegli, H., 2003. A multi-resolution ICP with heuristic closest point search for fast and robust 3D registration of range images. IEEE International Conference on 3D Digital Imaging and Modeling, Banff, October 6–10, pp. 427–433.

Maas, H.G., 1994. A high-speed solid state camera system for the acquisition of flow tomography sequences for 3D least squares matching. International Archives of Photogrammetry and Remote Sensing 30 (Part 5), 241–249.

Maas, H.G., 2001. On the use of pulse reflectance data for laserscanner strip adjustment. International Archives of Photogrammetry, Remote Sensing and Spatial Information Sciences 34 (Part 3/W4), 53–56.

Maas, H.G., 2002. Methods for measuring height and planimetry discrepancies in airborne laserscanner data. Photogrammetric Engineering and Remote Sensing 68 (9), 933–940.

Maas, H.G., Gruen, A., 1995. Digital photogrammetric techniques for high resolution three dimensional flow velocity measurements. Optical Engineering 34 (7), 1970–1976.

Neugebauer, P.J., 1997. Reconstruction of real-world objects via simultaneous registration and robust combination of multiple range images. International Journal of Shape Modeling 3 (1–2), 71–90.

Okatani, I.S., Deguchi, K., 2002. A method for fine registration of multiple view range images considering the measurement error properties. Computer Vision and Image Understanding 87 (1–3), 66–77.

Park, S.Y., Subbarao, M., 2003. A fast point-to-tangent plane technique for multi-view registration. IEEE International Conference on 3D Digital Imaging and Modeling, Banff, October 6–10, pp. 276–283.

Pulli, K., 1999. Multiview registration for large data sets. IEEE International Conference on 3D Digital Imaging and Modeling, Ottawa, October 4–8, pp. 160–168.

Roth, G., 1999. Registering two overlapping range images. IEEE International Conference on 3D Digital Imaging and Modeling, Ottawa, October 4–8, pp. 191–200.

Rusinkiewicz, S., Levoy, M., 2001. Efficient variants of the ICP algorithm. IEEE International Conference on 3D Digital Imaging and Modeling, Quebec, May 28–June 1, pp. 145–152.

Szeliski, R., Lavallee, S., 1996. Matching 3-D anatomical surfaces with non-rigid deformations using octree-splines. International Journal of Computer Vision 18 (2), 171–186.

Vanden Wyngaerd, J., Van Gool, L., 2003. Combining texture and shape for automatic crude patch registration. IEEE International Conference on 3D Digital Imaging and Modeling, Banff, Canada, October 6–10, pp. 179–186.

Weik, S., 1997. Registration of 3-D partial surface models using luminance and depth information. IEEE International Conference on Recent Advances in 3D Digital Imaging and Modeling, Ottawa, Canada, May 12–15, pp. 93–100.

Williams, J.A., Bennamoun, M., Latham, S., 1999. Multiple view 3D registration: a review and a new technique. IEEE International Conference on Systems, Man, and Cybernetics, Tokyo, October 12–15, pp. 497–502.

Yoshida, K., Saito, H., 2002. Registration of range images using texture of high-resolution color images. IAPR Workshop on Machine Vision Applications (MVA'02), Nara, December 11–13, pp. 150–153.

Zhang, Z., 1994. Iterative point matching for registration of free-form curves and surfaces. International Journal of Computer Vision 13 (2), 119–152.